Journal of Alloys and Compounds 787 (2019) 1349–1355

Contents lists available at ScienceDirect

Journal of Alloys and Compounds

journal homepage: http://www.elsevier.com/locate/jalcom

Combining solid state NMR, powder X-ray diffraction, and DFT calculations for $CsSc_3F_{10}$ structure determination

Aydar Rakhmatullin [a, *], Mathieu Allix [a], Ilya B. Polovov [b], Dmitry Maltsev [b], Andrey V. Chukin [c], Rinat Bakirov [d], Catherine Bessada [a]

[a] Conditions Extrêmes et Materiaux: Haute Température et Irradiation, CEMHTI, UPR 3079 -CNRS Univ Orleans, 45071, Orléans, France
[b] Department of Rare Metals and Nanomaterials, Institute of Physics and Technology Ural Federal University, Ekaterinburg, Russia
[c] Department of Theoretical Physics and Applied Mathematics, Ural Federal University, 19, Mira Str., 620002, Ekaterinburg, Russia
[d] Department of Technology of Mechanical Engineering and Instrument Making, Votkinsk Branch of Kalashnikov Izhevsk State Technical University, 1, Shuvalova Str., 427000, Votkinsk, Russia

ARTICLE INFO

Article history:
Received 14 October 2018
Received in revised form
25 January 2019
Accepted 28 January 2019
Available online 31 January 2019

Keywords:
Solid-state NMR
X-ray
CASTEP
Coordination number

ABSTRACT

A combination of high field solid-state MAS NMR spectroscopy, X-ray diffraction, and first-principles calculations is used to elucidate the crystalline structure of $CsSc_3F_{10}$. At room temperature, this phase was found to crystallize in the *Pmma* (n°51) space group with $a = 8.0837(1)$ Å, $b = 7.5764(1)$ Å, and $c = 6.8127(1)$ Å. The remarkable feature of $CsSc_3F_{10}$ is an unusual high cesium coordination number of 18. ^{45}Sc -^{19}F D-HMQC NMR method has been employed to investigate the connectivity of scandium with fluorine atoms. NMR parameters were determined using first principle DFT calculations and compared with experimentally obtained data.

1. Introduction

In recent years, alkali metal fluoroscandates have attracted a lot of attention due to their potential applications in solid-state lasers, solar cell, fluorescent probes and many other areas [1–5]. The necessary improvement of these different crystalline materials for these specific applications requires precise knowledge of the local structure and an accurate description of their structure. There are many reports on lithium, potassium, and sodium fluoroscandates (for example: $LiScF_4$ [5], KSc_2F_7 [2,3], $NaScF_4$ [1,2], and others [6]), but relatively little is known about rubidium- and cesium-containing fluoride compounds. We suppose that the main reasons for this lack of investigations are related to the high cost of ScF_3 and the high corrosiveness and hygroscopicity of Rb and Cs fluorides. In the CsF-ScF_3 system, only the structure of $CsScF_4$ has been reported [7].

Up to now, the crystal structure of $CsSc_3F_{10}$ remains unknown. Champarnaud-Mesjard and Frit [8] reported the synthesis of this material and proposed an orthorhombic symmetry and with a structure that might be isostructural with $RbIn_3F_{10}$ [9], which crystallizes in the $P222_1$ space group. In this model, indium atoms present two different kinds of coordination: In1 exhibits octahedral coordination whereas In2 and In3 are 7-coordinated with pentagonal bipyramid environments. All these fluorinated polyhedra sharing either edges or corners form a three dimensional framework, $(In_3F_{10})^-$, with tunnels parallel to the *z* axis where are located (8 + 2)-coordinated rubidium atoms. $CsSc_3F_{10}$ was reported to be stable up to 477 °C, temperature above which it decomposes into $CsScF_4$, and ScF_3.

Solid state NMR combined with theoretical frameworks, such as DFT calculations, becomes a more and more powerful tool for determining the structure of crystalline materials, complementing the usual diffraction techniques. This combined approach has found many applications for a wide range of materials [10–12]. In this work, we use such an approach to determine and describe finely the structure of $CsSc_3F_{10}$ by coupling X-ray diffraction, 1D and 2D D-HMQC solid-state NMR techniques and first principles calculations. The unusually high cesium coordination number in a pure fluorine 18 (12 + 6) environment is discussed in detail.

* Corresponding author.
E-mail address: rakhmat@cnrs-orleans.fr (A. Rakhmatullin).

https://doi.org/10.1016/j.jallcom.2019.01.355
0925-8388/

2. Experimental methods

2.1. Synthesis

Scandium fluoride was obtained by precipitation from a solution of scandium chloride using hydrofluoric acid. Scandium chloride solution was previously prepared by reacting scandium oxide (99.9%, Sigma-Aldrich) with hydrochloric acid (analytical purity). The precipitate was centrifuged and then air-dried at 130 °C. At the final stage, ScF_3 was dried under vacuum at 300 °C. The residual water content in ScF_3 samples was below 0.01 wt%. The mechanically homogenized powder mixture of CsF (99%, Sigma-Aldrich) and ScF_3, previously weighed in stoichiometric ratios to match the $CsSc_3F_{10}$ composition, was placed in a nickel crucible and heated from room temperature to 402 °C using a rate of 2 °C/min under argon atmosphere. The holding time was 100 hours and then the sample was cooled down to room temperature with an approximate rate of 2 °C/min.

2.2. NMR measurements

Solid state ^{19}F, ^{45}Sc, and ^{133}Cs NMR spectra were obtained using Bruker AVANCE III HD 750 (17.6 T) and 850 (20 T) NMR spectrometers. ^{19}F, ^{45}Sc, and ^{133}Cs chemical shifts were referenced to a $CFCl_3$, 0.11 M $ScCl_3$ solution in 0.05 M HCl, and 0.5 M CsCl solution, respectively. Room temperature MAS NMR spectra were acquired using 1.3 mm Bruker MAS probes. Data were collected at spinning frequencies ranging from 40 to 67 kHz $\pi/2$ pulse widths were 0.73 μs and 2.85 μs for ^{19}F and ^{45}Sc, respectively. In order to improve the resolution, we have used PISSARRO [13] ^{45}Sc and ^{19}F decoupling.

The $SR4^2_1$ recoupling pulses [14] in the dipolar $^{45}Sc(^{19}F)$ HMQC experiments [15] were applied with nutation frequencies $\nu(^{19}F) = 42.4$ kHz ($\pi/2$ pulse of 5.9 μs). The optimum DQ transfer was obtained for $\tau = 0.2$ ms, corresponding to 12 rotor periods (two $SR4^2_1$ super-cycles). The radio-frequency field on the ^{45}Sc channel was $\nu(^{45}Sc) = 100$ kHz, the spinning speed was 60 kHz and the spectral width in the direct dimension was set to 60 kHz. 1052 complex points were recorded with 512 transients, and in the indirect dimension, 90 t_1 increments. Phase sensitive detection in the indirect dimension was obtained using the States method [16]. The recycling delay was set to 0.5 s.

2.3. Powder X-ray diffraction

XRPD data were recorded on a Bragg Brentano D8 Advance Bruker diffractometer (CuK_α radiation) equipped with a LynxEye XE detector over an angular range of $5° < 2\theta < 130°$ using a 0.012° step size. Structural refinements of the $CsSc_3F_{10}$ material were realized using the Rietveld [17] method with the JANA2006 [18] software.

2.4. CASTEP calculations

First-principles calculations of NMR parameters were performed using the CASTEP NMR program [19] running in the Materials Studio 7.0 environment using the experimental geometries determined via diffraction methods, pseudopotentials calculated "on-the-fly", and the Perdew, Burke, and Ernzerhof (PBE) [20] functionals in the generalized gradient approximation (GGA). The gauge including projector augmented wave (GIPAW) [21,22] method implemented in CASTEP provides accurate computed values of the periodic system properties and its use is well-established in the solid-state NMR literature [23,24]. The cut-off energies were 600 eV and k-point spacing of 0.04 $Å^{-1}$. Calculations were carried out after a geometry optimization of all atom positions, keeping the experimental cell parameters and symmetry constraints. Optimized structure was obtained by minimizing the residual forces ($|F|_{max}$ below 10 meV/Å) for all atoms. To convert the calculated isotropic chemical shielding into isotropic chemical shift, the definition of calibration curve relating isotropic chemical shift and shielding is necessary. For ^{45}Sc and ^{19}F the relationship reported in our previous study [6] are: $\delta_{iso} = -0.852 \times \sigma_{iso} + 667.42$ and $\delta_{iso} = -0.589 \times \sigma_{iso} + 20.24$, respectively.

3. Results and discussions

3.1. X-ray powder diffraction and NMR spectroscopy

First, X-ray powder diffraction (XRPD) was performed to determine the nature of the synthesized phase corresponding to the $CsSc_3F_{10}$ nominal composition. Auto-indexing analysis of the room temperature XRPD pattern was performed using Dicvol [25] and Treor [26] indexing softwares. The results led to a similar solution with good reliability factors: an orthorhombic cell with $a = 8.08$ Å, $b = 7.58$ Å and $c = 6.81$ Å. A subsequent ICDD database search using close cell parameters (volume tolerance of 10%) and chemical restrictions (presence of alkali metals and fluorine) resulted in no match with any reported compound with similar cell parameters. A small amount of a secondary phase was identified as ScF_3 (ICSD 77071) [27]. After unsuccessful attempts to find isostructural phases in both ICSD and ICDD databases, solid-state NMR spectroscopy was applied to gain more information on this new crystalline phase.

The ^{19}F MAS NMR spectrum of $CsSc_3F_{10}$ contains five peaks (Fig. 1a). Accurate simulation of the spectrum, including all spinning sideband patterns, yielded integral intensity ratios of

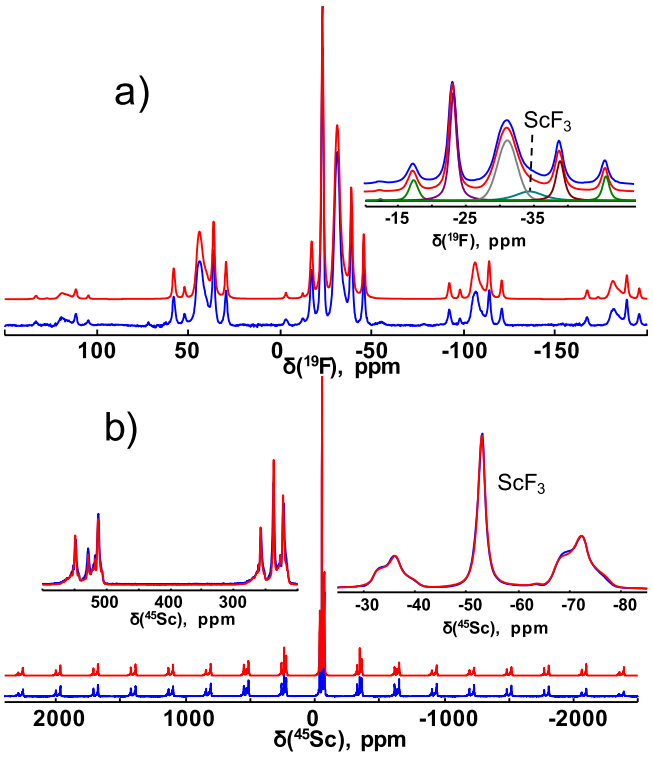

Fig. 1. ^{19}F (a) and ^{45}Sc (b) MAS NMR experimental (blue lines) spectra recorded at 60 kHz and at 20 T are presented with their simulations (red lines). Inserts show (a) Isotropic resonances of the ^{19}F spectrum and (b) expanded ^{45}Sc MAS spectrum in the region of the central transition (right); and expanded satellite transition sideband revealing their complex line shape (left). (For interpretation of the references to colour in this figure legend, the reader is referred to the Web version of this article.)

1:2:4:2:1 for the resonances at −17.1 ppm, −23.0 ppm, −31.0 ppm, −38.8 ppm, and −45.6 ppm, respectively (Table 1). The very small peak of maximum at −33.9 ppm [6] and showing a Lorentzian-Gaussian line shape, and was assigned to the secondary phase ScF_3. Additionally spectrum shows 3 very small peaks at −3.2 ppm, −12.5 ppm and −55 ppm. The integral intensities of these peaks were very small, i.e. 0.15%, 0.33%, and 0.24% respectively. We suppose that this is some unknown cesium fluoroscandates $Cs_xSc_yF_z$. The chemical shift for the bridging fluorine atoms is ranging from −23 to −75 ppm [6], therefore, it can be concluded that each fluorine atom in the $CsSc_3F_{10}$ compound is bonded with two scandium atoms.

^{45}Sc MAS NMR spectra recorded at 17.6 T and 20 T contains two typical quadrupolar lines with relative signal intensities of 1:2 (Table 2 and Fig. 1b and S1). The ^{45}Sc chemical shift values for six and seven coordinated scandium environments range from −20 to 14 ppm and from −53.5 to −40 ppm, respectively [6]. To the best of our knowledge, there are no NMR data available for the eight coordination scandium environment [5]. Therefore, from scandium NMR results, it is difficult to define exactly the coordination number of scandium atoms. Despite the isotropic chemical shift of the atoms resonating at a low frequency is beyond the range of sevenfold coordinated scandium, we suppose that they are most probably seven coordinated. However, the coordination number eight for these atoms cannot be excluded. The resonance at a higher frequency can be assigned to either a 6- or 7- fold coordination.

The presence of the secondary phase ScF_3 was also observed in ^{45}Sc NMR spectra. Due to the small deviation of local ^{45}Sc environment from perfect spherical symmetry in ScF_3, we observed at $\nu_{rot} = 60$ kHz a set of small spinning sideband patterns in the ^{45}Sc spectra. Almost all integral intensity is enclosed in an isotropic peak. It should be noted, that this peak is narrower compared to that of $CsSc_3F_{10}$, it has the Lorentzian-Gaussian line shape and FWHM = 300 Hz. In case of $CsSc_3F_{10}$, the integral intensity is distributed over the whole spectrum from −3000 ppm up to 3000 ppm. Additionally, the line shape of the signals of $CsSc_3F_{10}$ shows a quadrupolar broadening. High amplitude of ^{45}Sc NMR signal of ScF_3 compare to that of $CsSc_3F_{10}$ makes the impression that the content of scandium fluoride impurity in $CsSc_3F_{10}$ was significant.

In order to gain additional information about the chemical bonding between scandium and fluorine, we have performed ^{45}Sc-^{19}F D-HMQC MAS NMR experiment (Fig. 2). On the 2D map, one can observe spots corresponding to Sc–F bonds. It is seen that Sc1 type atom is connected with fluorine sites of only two types.

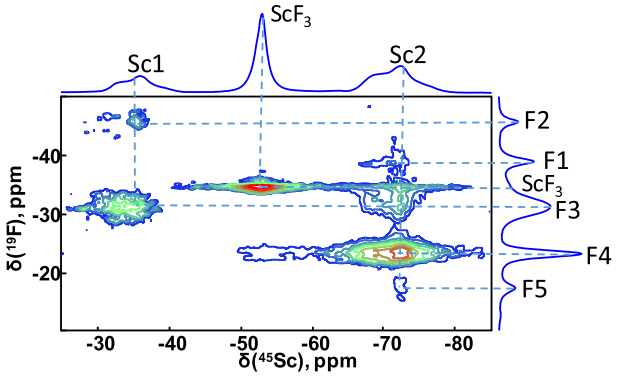

Fig. 2. ^{45}Sc -^{19}F D-HMQC NMR spectrum recorded at spinning frequency of 60 kHz and at 20 T. Dashed lines show a correlation between fluorine and scandium atoms.

The integral intensities of two 2D peaks of Sc1 type atoms are different; it means that Sc1 atom is more strongly bonded (with a shorter bond length) with the fluorine site resonating at −31 ppm or that out of six/seven fluorine sites surrounding Sc1 atom, more fluorine sites resonate at −31 ppm than at −45.6 ppm. Second type scandium atom (Sc2) is surrounded by four different fluorine sites. We note that the spot Sc2 with F at 23 ppm has the highest integral intensity.

The ^{133}Cs spectrum recorded at 20 T and 60 kHz exhibits only one resonance with a Gaussian line shape and a maximum at −1.2 ppm and FWHM = 200 Hz (Fig. 2S). This observation indicates the existence of only one type of symmetrical environment for cesium atoms, even though fast exchange in NMR time scale between few cesium sites cannot be excluded.

3.2. Determination of the crystal structure of $CsSc_3F_{10}$

As stated above no isostructural model could be found in the ICDD database to match the cell ($a = 8.08$ Å, $b = 7.58$ Å and $c = 6.81$ Å) determined by auto-indexation. However, an extensive bibliographic search allowed us to find a PhD dissertation mentioning the structure of $RbSc_3F_{10}$ [28]. The proposed model of $RbSc_3F_{10}$ (*Pmma*, $a = 7.790$ Å, $b = 7.581$ Å and $c = 6.648$ Å) contains five crystallographically nonequivalent bridging F sites with relative multiplicities of 2:4:8:4:2, two Sc sites with relative multiplicities of 1:2, and one Rb site. This description perfectly matches our NMR results, and thus indicates that $CsSc_3F_{10}$ could be isostructural to $RbSc_3F_{10}$.

Table 1
Experimental (isotropic chemical shifts δ_{iso}, chemical shift anisotropies Δ, asymmetry parameters η_{cs}, integral intensities I) and calculated (isotropic magnetic shielding σ_{iso} and isotropic chemical shifts $\delta_{calciso}$) ^{19}F NMR parameters.

Fluorine site	δ_{iso}, ppm (±0.1 ppm)	Δ, ppm (±10 ppm)	η_{cs} (±0.1)	I, % (±1%)	σ_{iso}, ppm	$\delta_{calciso}$, ppm
F5	−17.1	−167	0.24	10	72.3	−22.4
F4	−23.0	−53	0.03	20	96.9	−36.9
F3	−31.0	−141	0.02	40	100.2	−38.8
F1	−38.8	−181	0.26	20	107.2	−42.9
F2	−45.6	−168	0.2	10	118.0	−49.3

Table 2
^{45}Sc isotropic chemical shifts (δ_{iso}), quadrupolar constants (C_Q), asymmetry parameters (η_Q), and Integral intensities (I) obtained from the simulation of the ^{45}Sc MAS at 17.6 T and 20 T and calculated ^{45}Sc NMR parameters (isotropic magnetic shielding σ_{iso}, $|C_{Qcalc}|$ quadrupolar constant, and η_{Qcalc} asymmetry parameter).

Atom	δ_{iso}, ppm (±0.2 ppm)	C_Q, MHz (±0.1 MHz)	η_Q (±0.1)	I, % (±1%)	σ, ppm	$\delta_{iso\ calc}$, ppm	$\lvert C_{Qcalc}\rvert$, MHz	η_{Qcalc}
Sc1	−32.2	7.4	0.8	33	831.8	−33.9	7.4	0.33
Sc2	−67.3	8.1	0.8	67	861.6	−55.4	7.4	0.94

In order to determine precisely the structure of $CsSc_3F_{10}$, a Rietveld refinement of room temperature XRPD data was performed. The starting model was based on the $RbSc_3F_{10}$ structure using the $CsSc_3F_{10}$ cell parameters previously determined and substituting Cs for Rb. Both cationic and fluorine positions, as well as atomic displacement parameters, were refined. Good reliability factors were obtained (wRp = 6.00%, Rp = 3.48% and GOF = 7.21). The fit of the XRPD Rietveld refinement is shown in Fig. 3. Crystallographic data, atomic coordinates, atomic displacement parameters and Cs–F and Sc–F interatomic distances are summarized in Tables 3–5. The amount of the secondary phase ScF_3 was estimated at about 6.6 wt% and 6.3 wt% from powder XRD and ^{19}F NMR, respectively.

The Sc atoms in $CsSc_3F_{10}$ present two different kinds of coordination environments, as well as in $RbSc_3F_{10}$ [28]: 1/3 of the Sc atoms (Sc1) occupy slightly distorted octahedra and 2/3 (Sc2) occupy pentagonal bipyramids (Figs. 4 and 5). The structure is formed by the insertion of octahedral chains between parallel sheets of pentagonal bipyramids. The bipyramids share edges and vertices in the *c* direction and vertices only along the *a* direction. The hexagonal tunnels formed in the three-dimensional framework are occupied by Cs atoms. It should be noted that Cs atoms are situated in the tunnel central axis along the *a*-axis.

The coordination environments of the scandium and cesium atoms are shown in Fig. 5. F3 fluorine atoms form the octahedron's base of Sc1 and two F2 atoms are located in the apex. The Sc1–F2/F3 distances are almost equivalent, 2.021(1) Å and 2.008(3) Å respectively, and they are very close to the value reported for ScF_3 (2.01 Å) [27]. The octahedral environment around Sc1 exhibits F2–Sc1–F2 bond angles of 180° and small deviations from ideal octahedral angles are observed in the F3–Sc1–F3 bond angles, which are 180° and 90° ±2.90°. Sc2 is coordinated to seven fluorine atoms. The average Sc2–F distance in the pentagonal bipyramid is 2.07(2) Å. Sc2 occupies the centre of a distorted pentagonal bipyramid with F1–Sc2–F1 angles of 178.58°. The two distinct Sc-centered polyhedra are joined together through F3 bonding. The connections between the Sc-centered polyhedra between the different layers are indicated by bond angles of 178.07° and 175.16°, for Sc1–F2–Sc1 and Sc2–F1–Sc2 respectively. Cesium is sandwiched by two slightly distorted hexagonal F planes with bond distances ranging from 2.95(2) Å to 3.42(2) Å (12 coordination). Four additional F1 atoms from the vertices of the pentagonal bipyramids and two additional F2 atoms from the vertices of the octahedra are located at longer distances of 3.76(2), 3.89(2) Å and 3.79(2), respectively (Figs. 4 and 5, Table 5). The average Cs–F distance is 3.45 Å. Therefore, cesium exhibits an unusual high coordination number of 18, which can also be noted as 12 + 6, as 6 Cs–F distances are above 3.5 Å.

Cesium usually show a variable coordination environment ranging from 6 to 12 [29], but it can also form complexes with unusually high coordination numbers above twelve. However, such a coordination number is rare because of the limited space available around the alkali atom. Pollak et al. studied $Cs[H_2NB_2(C_6F_5)_6]$ metallocomplexe, in which a central cesium atom is coordinated by 16 fluorine atoms [30]. To the best of our knowledge, this was the highest cesium coordination number reported to date. In this metallocomplexe structure, eight Cs–F distances range between 3.099(3) and 3.303(3) Å and eight more distances are above 3.5 Å, ranging between 3.569(2) and 3.799(1) Å, with a mean distance of 3.423 Å. Thus, all bond distances values, as well as, the average value are very close to that observed in $CsSc_3F_{10}$. In the isostructural $RbSc_3F_{10}$ structure, the angles between the Sc-centered polyhedra of the different layers are of 157.60° and 161.75°, for Sc1–F2–Sc1 and Sc2–F1–Sc2 respectively. The polyhedra of each layer are more inclined relatively to each other. This leads to a change in the distances between alkali metal and transition metal/fluorine, d(Rb–Sc2) = 4.283(6) Å and d(Rb–F1) = 4.056(5) Å, d(Rb–F2) = 3.804(3) Å, respectively, which are almost identical. Only two additional F1 atoms from the vertices of the pentagonal bipyramids are bonded to the Rb atom at a distance 3.393(5) Å. It should be noted that the rubidium cation has smaller ionic radius than cesium cation. Consequently, rubidium atom in $RbSc_3F_{10}$ is only 14 coordinated, whereas cesium is 18-coordinated in $CsSc_3F_{10}$ [28].

$CsSc_3F_{10}$, as well as $RbSc_3F_{10}$, has a structure similar to that of

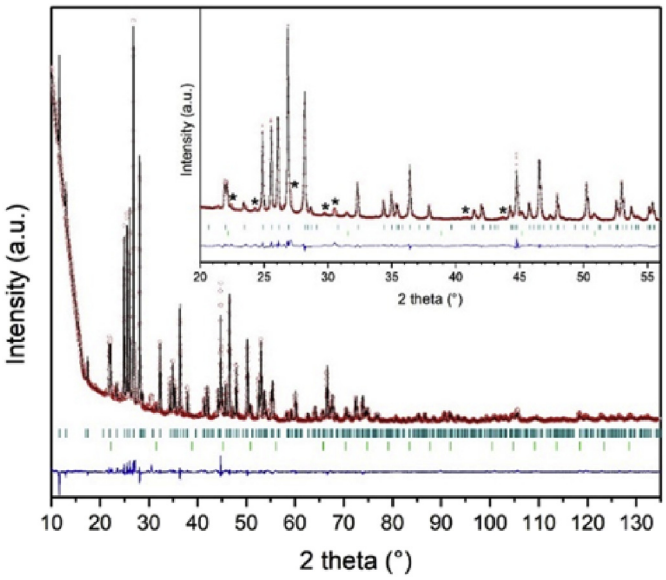

Fig. 3. Experimental (red), calculated (black) and difference (blue) XRPD Rietveld refinement of $CsSc_3F_{10}$ (green marks). Insert shows expanded area between 20 and 56°. Final reliability factors are wRp = 6.00%, Rp = 3.48% and GOF = 7.21. Light green marks correspond to the secondary phase ScF_3. (For interpretation of the references to colour in this figure legend, the reader is referred to the Web version of this article.)

Table 3
Crystallographic data from XRD Rietveld refinement.

Chemical formula	$CsSc_3F_{10}$
Formula weight ($g.mol^{-1}$)	457.8
Temperature, °C	20
Z	2
Crystal system	Orthorhombic
Space group	*Pmma* (n°51)
Unit cell dimensions, Å	$a = 8.0837(1)$
	$b = 7.5764(1)$
	$c = 6.8127(1)$
Cell volume ($Å^3$)	417.25(1)
Density, calculated ($g.cm^{-3}$)	3.644

Table 4
Atomic coordinates, occupancy *(Occ)* and equivalent isotropic displacement parameters (U_{eq}) ($Å^2 \times 10^3$).

Atom	Site	X	Y	Z	*Occ*	U_{eq}
Cs1	2e	1/4	0	0.501(1)	1	0.034(5)
Sc1	2d	0	1/2	1/2	1	0.031(1)
Sc2	4g	0	0.2342(3)	0	1	0.018(1)
F1	4k	1/4	0.2309(7)	0.012(3)	1	0.016(2)
F2	2f	1/4	1/2	0.495(8)	1	0.028(3)
F3	8l	0.007(3)	0.308(1)	0.7028(5)	1	0.034(2)
F4	4i	−0.015(2)	0	0.830(1)	1	0.023(2)
F5	2b	0	1/2	0	1	0.044(3)

Table 5
Selected bond lengths (Å) from XRD Rietveld refinement.

Sc1–F2 × 2 2.021(1)	Sc2–F1 × 2 2.023(1)	Cs1–F3 × 4 3.35(2)	Cs1–F1 × 2 3.76(2)
Sc1–F3 × 4 2.008(3)	Sc2–F3 × 2 2.101(3)	Cs1–F3 × 4 3.42(2)	Cs1-F1 × 2 3.89(2)
	Sc2–F4 × 2 2.121(3)	Cs1–F4 × 2 2.95(2)	Cs1–F2 × 2 3.79(1)
	Sc2–F5 × 1 2.013(2)	Cs1–F4 × 2 3.10(2)	

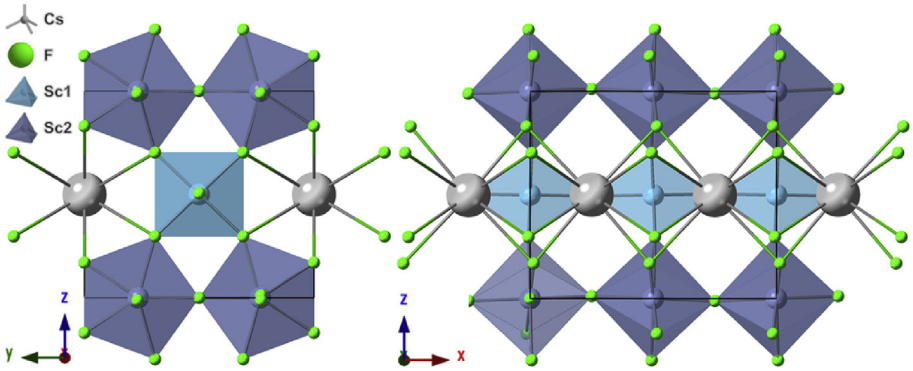

Fig. 4. Layer structure viewed along *x*-axis and *y*-axis.

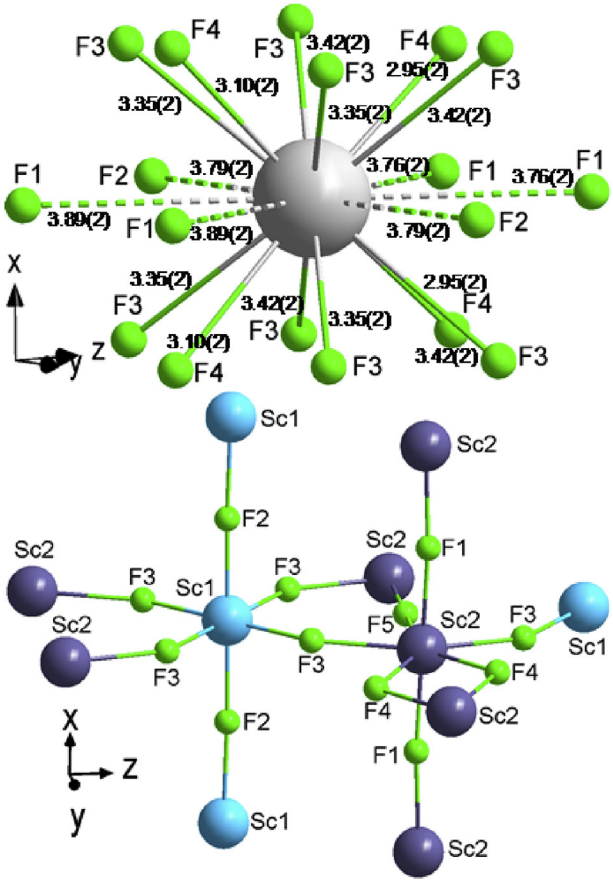

Fig. 5. Coordination environments of rubidium and scandium atoms. Dashed lines show Cs-F bonds longer than 3.5 Å. Cs-F bonds distances in Å.

$RbIn_3F_{10}$, but the cesium and rubidium compositions are characterized by a higher symmetry, *Pmma* space group, than $RbIn_3F_{10}$ ($P222_1$). In all three compounds, the chains of pentagonal bipyramids are linked by the vertices constituting sheets parallel to the *xoz* plane. These sheets are interconnected by vertex-sharing octahedra. The three-dimensional network contains fluorinated tunnels parallel to the *z* axis, into the alkali atoms are inserted. The coordination environments of indium atoms in $RbIn_3F_{10}$ are more distorted, which leads to the presence of two kinds of sevenfold coordinated indium atoms with multiplicities of 1:1, and also to different coordination environments for rubidium. The coordination of each rubidium atom is 8 + 2: two F4 atoms are situated at distances d(Rb-F4) = 3.37 Å, than the other eight are located at distances from 2.77 Å to 3.13 Å. These eight fluorine atoms are situated approximately at the vertices of a dodecahedron.

3.3. CASTEP data

After the crystal structure determination by XRPD, CASTEP calculations were performed on the (atomic positions) optimized structure. The geometry optimization leads to only very small shifts in atomic coordinates ($|\Delta x|$, $|\Delta y|$, $|\Delta z| \leq 0.0103$ or |atomic displacements| ≤ 0.0851 Å; Table 1S). Therefore, the crystal structure determined from the XRPD data is close to the minimum energy structure. It should be noted that the obtained values of the atomic displacements are close to those found for the structure determined from powder XRD, i.e. up to 0.0131 Å for $K_5Sc_3F_{14}$ [6] and up to 0.125 Å for K_2YF_5 and β-KY_2F_7 [31]. First-principles calculated ^{19}F and ^{45}Sc NMR parameters are given in Tables 1 and 2 along with the experimental results. A complete unambiguous assignment of ^{19}F resonances to fluorine crystallographic sites cannot be performed, if only the analysis of integral intensities is taken into account: the signals at −23.0 ppm, −38.8 ppm on the one hand and at −17.1 ppm, −45.6 ppm one the other have the same integral intensities. Based on relative intensities, an only partial assignment of the ^{19}F resonances to the F sites can be performed: lines at −17.1 ppm and at −45.6 ppm to F2 or F5; lines at −23.0 ppm and at −38.8 ppm to F1 or F4; line at −37.1 ppm to F3. Thus, the complete assignment of ^{19}F resonances to fluorine crystallographic sites was based on DFT computations, where the NMR lines were ranked by increasing order of experimental δ_{iso} values while the corresponding F sites were ranked by increasing order of calculated ^{19}F δ_{iso} values. This assignment of lines to F sites agrees well with the measured integral intensities (Table 1). We also note that this

assignment is in a very good agreement with ^{45}Sc-^{19}F D-HMQC spectrum: Sc1 atom is bonded to F3 and F2, and Sc2 is surrounded by F1, F3-F5. A discrepancy of *ca.* 14 ppm between experimental and calculated chemical shift values is observed for F4. The linear regression employed here was defined in the previous work [6] using data for lithium, sodium, and potassium fluoroscandates; no data for cesium fluoroscandates were available. Since F4 is the fluorine atom closest to the cesium atom (Table 5), we may attribute the discrepancy to an imperfect description of the ultrasoft pseudopotentials (USPP) of cesium. Similar discrepancy was also observed in case of CsF [32]. The attribution of ^{45}Sc signals was performed from the integral intensities. The resonance with integral intensity of 33% corresponds to Sc1 atom and the signal with 67% to Sc2 atom. The computed results agree well with the experimental data. The calculated C_Q for Sc2 atom is 7.4 MHz, and it is found slightly lower than the experimental one 8.1 MHz. There is difference between calculated and observed asymmetry parameter η_Q for Sc1 site; the calculated values are higher, 0.8 and 0.33, respectively. A possible reason for this ambiguity is that accurate calculations of η_Q value require a high precision on the determination of all three EFG tensor components V_{xx}, V_{yy} and V_{zz}. However, the agreement between all calculated and experimental NMR parameters is satisfying and enables reliable assignment of the observed experimental resonances.

4. Conclusions

$CsSc_3F_{10}$ was synthesized by a solid state reaction route. It was structurally characterized using a combination of high field solid-state MAS NMR spectroscopy, X-ray diffraction, and first-principles calculations. $CsSc_3F_{10}$ exhibits an orthorhombic structure that is built by stacking layers of Sc-centered polyhedra. The resulting frameworks contain tunnels that are filled by the cesium atoms. An unusual high cesium coordination number of 18 (12 + 6) was observed. It is the highest coordination for cesium reported to date. NMR parameters were determined using first principle DFT calculations. These results could be useful for further designing novel fluoroscandate's materials with industrial and scientific applications.

Acknowledgment

This work was supported by the Ministry of Education and Science of the Russian Federation N№02.G25.31.0210 of 27.04.2016. Financial support from the TGIR-RMN-THC Fr3050 CNRS for conducting the research is gratefully acknowledged. For the calculations, we thank the “Centre de Calcul Scientifique en region Centre” (Orleans, France).

Appendix A. Supplementary data

Supplementary data to this article can be found online at https://doi.org/10.1016/j.jallcom.2019.01.355.

References

[1] Y. Ai, D. Tu, W. Zheng, Y. Liu, J. Kong, P. Hu, Z. Chen, M. Huang, X. Chen, Lanthanide-doped $NaScF_4$ nanoprobes: crystal structure, optical spectroscopy and biodetection, Nanoscale 5 (2013) 6430–6438. https://doi.org/10.1039/C3NR01529G.

[2] B. Yu, E. Hao, S. Fang, Z. Liu, Y. Wang, Z. Lv, N. Li, X. Zhang, L. Shi, Y. Du, Controlled synthesis of high quality scandium-based nanocrystals as promising recyclable catalysts for silylcyanation reaction, Nanoscale 9 (2017) 10987–10991. https://doi.org/10.1039/C7NR04408A.

[3] J. Xiong, J. Yu, Y. Zhang, W. Xia, S. Hu, Y. Zhang, J. Yang, One-step surfactant-free synthesis of KSc_2F_7 microcrystals: controllable phases, rich morphologies and multicolor down conversion luminescence properties, CrystEngComm 20 (2018) 3978–3986. https://doi.org/10.1039/C8CE00716K.

[4] L. Zhang, S. Zhao, Z. Liang, J. Zhang, W. Zhu, P. Liu, H. Sun, The colour tuning of upconversion emission from green to red in $NaScF_4$:Yb^{3+}/Er^{3+} nanocrystals by adjusting the reaction time, J. Alloys Compd. 699 (2017) 1–6. https://doi.org/10.1016/j.jallcom.2016.12.202.

[5] A.K. Tyagi, J. Köhler, P. Balog, J. Weber, Syntheses and structures of Li_3ScF_6 and high pressure $LiScF_4$, luminescence properties of $LiScF_4$, a new phase in the system LiF–ScF_3, J. Solid State Chem. 178 (2005) 2620–2625. https://doi.org/10.1016/j.jssc.2005.04.038.

[6] A. Rakhmatullin, I.B. Polovov, D. Maltsev, M. Allix, V. Volkovich, A.V. Chukin, M. Boča, C. Bessada, Combined approach for the structural characterization of alkali fluoroscandates: solid-state NMR, powder X-ray diffraction, and density functional theory calculations, Inorg. Chem. 57 (2018) 1184–1195. https://doi.org/10.1021/acs.inorgchem.7b02617.

[7] A.S. Krylov, M.S. Molokeev, S.V. Misyul, S.N. Krylova, A.S. Oreshonkov, A.A. Ivanenko, V.A. Zykova, Y.N. Ivanov, A.A. Sukhovsky, V.N. Voronov, I.N. Safonov, A.N. Vtyurin, Crystal structure and phase transitions of a layered perovskite-like $CsScF_4$ crystal, CrystEngComm 18 (2016) 8472–8486. https://doi.org/10.1039/C6CE01144F.

[8] J.-C. Champarnaud-Mesjard, B. Frit, Les systemes MF-ScF_3 (M = Li, Na, K, Rb, Cs, Tl, NH_4), J. Less Common. Met. 167 (1991) 319–327. https://doi.org/10.1016/0022-5088(91)90284-B.

[9] J.C. Champarnaud-Mesjard, D. Mercurio, B. Frit, Structure cristalline du fluoroindate de rubidium $RbIn_3F_{10}$, J. Inorg. Nucl. Chem. 39 (1977) 947–951. https://doi.org/10.1016/0022-1902(77)80241-8.

[10] C. Martineau, M. Allix, M.R. Suchomel, F. Porcher, F. Vivet, C. Legein, M. Body, D. Massiot, F. Taulelle, F. Fayon, Structure determination of Ba_5AlF_{13} by coupling electron, synchrotron and neutron powder diffraction, solid-state NMR and ab initio calculations, Dalton Trans. 45 (2016) 15565–15574. https://doi.org/10.1039/C6DT02454H.

[11] C. Martineau, J. Senker, F. Taulelle, Chapter one - NMR crystallography, in: G.A. Webb (Ed.), Ann. R. NMR S., Academic Press, 2014, pp. 1–57. https://doi.org/10.1016/B978-0-12-800184-4.00001-1.

[12] A.-L. Rollet, M. Allix, E. Veron, M. Deschamps, V. Montouillout, M.R. Suchomel, E. Suard, M. Barre, M. Ocaña, A. Sadoc, F. Boucher, C. Bessada, D. Massiot, F. Fayon, Synthesis and structure resolution of $RbLaF_4$, Inorg. Chem. 51 (2012) 2272–2282. https://doi.org/10.1021/ic202301e.

[13] M. Weingarth, G. Bodenhausen, P. Tekely, Probing the quenching of rotary resonance by PISSARRO decoupling, Chem. Phys. Lett. 502 (2011) 259–265. https://doi.org/10.1016/j.cplett.2010.12.040.

[14] A. Brinkmann, A.P.M. Kentgens, Proton-Selective ^{17}O–H distance measurements in fast magic-angle-spinning solid-state NMR spectroscopy for the determination of hydrogen bond lengths, J. Am. Chem. Soc. 128 (2006) 14758–14759. https://doi.org/10.1021/ja065415k.

[15] J. Trebosc, B. Hu, J.P. Amoureux, Z. Gan, Through-space R3-HETCOR experiments between spin-1/2 and half-integer quadrupolar nuclei in solid-state NMR, J. Magn. Reson. 186 (2007) 220–227. http://doi.org/10.1016/j.jmr.2007.02.015.

[16] D.J. States, R.A. Haberkorn, D.J. Ruben, A two-dimensional nuclear overhauser experiment with pure absorption phase in four quadrants, J. Magn. Reson. (1969) 48 (1982) 286–292. https://doi.org/10.1016/0022-2364(82)90279-7.

[17] H. Rietveld, A profile refinement method for nuclear and magnetic structures, J. Appl. Crystallogr. 2 (1969) 65–71. https://doi.org/10.1107/S0021889869006558.

[18] V. Petříček, M. Dušek, L. Palatinus, Crystallographic computing system JANA2006: General features, Z. Kristallogr. 229 (2014) 345. https://doi.org/10.1515/zkri-2014-1737.

[19] M.D. Segall, C.J. Pickard, P.J. Hasnip, M.J. Probert, K. Refson, M.C. Payne, First principles methods using CASTEP, Z. Kristallogr. 220 (2005) 567–570. https://doi.org/10.1524/zkri.220.5.567.65075.

[20] J.P. Perdew, K. Burke, M. Ernzerhof, Generalized Gradient approximation made simple, Phys. Rev. Lett. 77 (1996) 3865–3868. https://doi.org/10.1103/PhysRevLett.77.3865.

[21] J.R. Yates, C.J. Pickard, F. Mauri, Calculation of NMR chemical shifts for extended systems using ultrasoft pseudopotentials, Phys. Rev. B 76 (2007), 024401. https://doi.org/10.1103/PhysRevB.76.024401.

[22] C.J. Pickard, F. Mauri, All-electron magnetic response with pseudopotentials: NMR chemical shifts, Phys. Rev. B 63 (2001), 245101. https://doi.org/10.1103/PhysRevB.63.245101.

[23] T. Charpentier, The PAW/GIPAW approach for computing NMR parameters: A new dimension added to NMR study of solids, Solid State Nucl. Magn. Reson. 40 (2011) 1–20. https://doi.org/10.1016/j.ssnmr.2011.04.006.

[24] C. Bonhomme, C. Gervais, F. Babonneau, C. Coelho, F. Pourpoint, T. Azaïs, S.E. Ashbrook, J.M. Griffin, J.R. Yates, F. Mauri, C.J. Pickard, First-principles calculation of NMR parameters using the gauge including projector augmented wave method: A chemist's point of view, Chem. Rev. 112 (2012) 5733–5779. https://doi.org/10.1021/cr300108a.

[25] A. Boultif, D. Louer, Indexing of powder diffraction patterns for low-symmetry lattices by the successive dichotomy method, J. Appl. Crystallogr. 24 (1991) 987–993. https://doi.org/10.1107/S0021889891006441.

[26] P.-E. Werner, Trial-and-error computer methods for the indexing of unknown powder patterns, Z. Kristallogr. 120 (1964) 375–387. https://doi.org/10.1524/zkri.1964.120.4-5.375.

[27] P.P. Fedorov, V. Trnovcová, G.I. Kocherba, B.P. Sobolev, Ionic conductivity and dielectric relaxation of scandium fluoride, Crystallogr. Rep. 40 (1995)

663–666.
[28] Y. Yin, Ph.D. Thesis, in: New Solid-State Fluorides: Synthesis, Crystal Chemistry, and Optical Properties, Oregon State University, Oregon, USA, 1993, p. 143.
[29] R. Shannon, Revised effective ionic radii and systematic studies of interatomic distances in halides and chalcogenides, Acta Crystallogr. Sect. A 32 (1976) 751–767. https://doi.org/10.1107/S0567739476001551.
[30] D. Pollak, R. Goddard, K.-R. Pörschke, Cs[$H_2NB_2(C_6F_5)_6$] Featuring an unequivocal 16-coordinate cation, J. Am. Chem. Soc. 138 (2016) 9444–9451. https://doi.org/10.1021/jacs.6b02590.
[31] J. Dabachi, M. Body, J. Dittmer, A. Rakhmatullin, F. Fayon, C. Legein, Insight into the factors influencing NMR parameters in crystalline materials from the KF–YF_3 binary system, Dalton Trans. 48 (2019) 587–601. https://doi.org/10.1039/C8DT03241F.
[32] A. Sadoc, M. Body, C. Legein, M. Biswal, F. Fayon, X. Rocquefelte, F. Boucher, NMR parameters in alkali, alkaline earth and rare earth fluorides from first principle calculations, Phys. Chem. Chem. Phys. 13 (2011) 18539–18550. https://doi.org/10.1039/C1CP21253B.